AIAA JOURNAL
Vol. 47, No. 12, December 2009

Optimal Design of Constrained-Layer Damping Structures Considering Material and Operational Condition Variability

Byung C. Jung*
University of Maryland, College Park, Maryland 20742
Doo-Ho Lee†
Dongeui University, Busan 614-714, Republic of Korea
and
Byeng D. Youn‡
University of Maryland, College Park, Maryland 20742

DOI: 10.2514/1.43551

Surface damping treatment is a typical way to reduce noise and vibration of structures. The damping performance of a surface treatment is highly sensitive to the variability in operational temperature. This paper proposes a statistical approach to model the variability of viscoelastic damping material in a constrained-layer damping layout, to predict variability in the dynamic responses of viscoelastic damping material, and to obtain an optimal robust layout that accounts for severe variability in operational temperature. The viscoelastic damping material property can be modeled as a sum of 1) a random complex modulus due to operational temperature variability and 2) experiment/model errors in the complex modulus. The eigenvector dimension reduction method is used in probability analysis to predict the variability in the dynamic responses of the viscoelastic damping material. It is concluded that temperature variability is strongly propagated to that in the dynamic responses of the damping material. This study also performs reliability-based design optimization for an optimal robust design of the constrained-layer damping structure. It is shown that reliability-based design optimization gives a more robust and reliable damping layout design amidst severe variability in operational temperature.

Nomenclature

$\mathbf{A}$	=	covariance matrix
a_0	=	material parameter of the fractional derivative model
a_1	=	material parameter of the fractional derivative model
$\mathbf{b}$	=	design variable vector
c_1	=	material parameter of the fractional derivative model
d_1	=	material constant of the Arrhenius equation
E	=	expectation operator
E_1^*	=	random complex modulus
E^*	=	complex modulus
E'	=	storage modulus
E''	=	loss modulus
$\mathbf{e}$	=	vector of residual
$f\alpha$	=	reduced frequency
G	=	constraint function
G^t	=	target constraint value
H_1	=	thickness of the damping layer
H_2	=	thickness of the constraining layer
i	=	$\sqrt{-1}$
$\mathbf{K}$	=	global stiffness matrix of the beam finite element model
$\mathbf{k}$	=	generalized modal stiffness
L	=	length of the damping/constraining layer
$\mathbf{M}$	=	global mass matrix of the beam finite element model
m	=	generalized modal mass
N	=	number of random variables
P	=	probability
p	=	probability distribution function
q	=	number of test data
R^t	=	target reliability value
SS_E	=	residual sum of squares
s	=	standard deviation
s_T	=	standard deviation of temperature distribution
$\tilde{s}^2$	=	unbiased estimator of variance
T	=	temperature
$\mathbf{v}$	=	eigenvector
W	=	weight of damping and constraining layers
w	=	density of damping and constraining layers
$\mathbf{X}$	=	random variable vector
Y	=	statistical moment of the response
$\mathbf{y}$	=	complex eigenvector of the beam finite element model
z_i	=	observed value for residual sum of squares
$\hat{z}_i$	=	fitted value for residual sum of squares
a	=	shift factor
β	=	material parameter of the fractional derivative model
δ_{ij}	=	Kronecker delta
$\tilde{\varepsilon}$	=	strain
ε_E^*	=	noise in the complex modulus
ζ	=	point receptance frequency response function
η_k	=	modal loss factor of the kth mode of the beam finite element model
λ	=	eigenvalue
λ^c	=	complex eigenvalue of the beam finite element model
μ_T	=	mean of temperature distribution
ξ	=	width of the beam structure
ρ	=	correlation coefficient
$\tilde{\sigma}$	=	stress
ψ_k	=	natural frequency of the kth mode of the beam finite element model

Presented as Paper 5865 at the 12th AIAA/ISSMO Multidisciplinary Analysis and Optimization Conference, Victoria, British Columbia, Canada, 10–12 September 2008; received 31 January 2009; revision received 3 July 2009; accepted for publication 23 July 2009.

*Graduate Student, Department of Mechanical Engineering; bcjung@umd.edu.

†Associate Professor, Department of Mechanical Engineering, 995 Eomgwangno, Busanjin-gu; dooho@deu.ac.kr (Corresponding Author).

‡Assistant Professor, Department of Mechanical Engineering; bdyoun@umd.edu. Member AIAA (Cocorresponding Author).

I. Introduction

ADDING a viscoelastic damping material to a structural surface is a typical way to reduce noise and vibration of structures [1]. For example, damping sheets on the body of passenger cars reduce noise and vibration in the cabin. Damping materials are also used in airplanes, launching vehicles, ships, and electric appliances. In these applications, it is important to optimize the layout of the unconstrained/constrained-layer damping material to reduce vibration and noise of structures effectively. The optimization generally determines the optimal location and dimensions of damping sheets in view of damping efficiency and/or material cost.

It is difficult to obtain a robust damping layout design, since the viscoelastic damping material possesses frequency- and temperature-dependent dynamic responses. In most cases surface damping treatments are exposed to an open air, so the damping material experiences a wide range of temperatures, which vary periodically and randomly. As a result, substantial variations in the damping material properties can be observed in the service life of the material and are expected to reduce the quality of damping performance against noise and vibration. On the other hand, test data inherently contain experimental errors (e.g., experimental noise and measurement errors) due to difficulty in measuring the dynamic responses of the viscoelastic damping material. For example, the loss factor, which is one of the material properties, can be obtained by measuring time or frequency responses in a simple beam test. The loss factor is highly sensitive to the boundary conditions of a measurement apparatus, resulting in significant experimental error. The loss factor estimation is known to be the least accurate among the modal parameters of a structure [2]. A fractional derivative model is often used to describe frequency- and temperature-dependent dynamic characteristics of the damping material with a few parameters. Although the fractional derivative model is one of the best-known mathematical models, model error (or uncertainty) is inevitable.

Many researchers have suggested different optimal design formulations for damping layout of structures [3–10]. Studies have primarily focused on designing a constrained-layer damping layout to maximize damping efficiency. One of the authors of this paper also proposed design optimization methods for constrained/unconstrained-layer damping layouts in structural noise and vibration problems, in which the frequency- and temperature-dependent dynamic responses of the viscoelastic damping material were considered [11,12]. However, in these previous works the optimal damping layouts were obtained with no consideration of temperature variation and damping material uncertainty. Only a few researchers have acknowledged the importance of these factors to random damping characteristics in structural dynamic problems [13–16]. To the authors' knowledge, no systematic approach has been proposed to deal with the variability in the dynamic responses of the viscoelastic damping material in a design process.

This paper proposes a sound statistical approach to optimize a constrained-layer damping structure while considering the variability in the damping material properties due to operational temperature, experimental errors, and model error. In Sec. II, a constrained-layer damping beam model and the fractional derivative model are briefly explained as mathematical models for constrained-layer damping analysis. The fractional derivative model predicts frequency- and temperature-dependent dynamic responses of the damping material. Section III presents a statistical approach for variability characterization of the viscoelastic damping material (e.g., ISD-110 [17]). Variability of the damping material is decomposed into two parts: 1) a random complex modulus considering operational temperature variability and 2) the experimental/model errors in the complex modulus. In Sec. IV, reliability-based design optimization (RBDO) is carried out to find an optimal robust design of the constrained-layer damping structure. The eigenvector dimension reduction (EDR) method [18,19] is used for the probability analysis. It is shown that the proposed statistical approach gives robust and reliable damping layout design that considers variability in the viscoelastic damping material properties and operational temperatures.

II. Finite Element Analysis of Constrained-Layer Damping Structure

A. Finite Element Analysis

The constrained-layer damping beam in this work consists of three layers: the base beam, the viscoelastic damping layer, and the constraining layer. It is assumed that the three layers are bonded perfectly. To compute vibrational responses of the constrained-layer damping beam, a 10-DOF finite element formulation was developed, as shown in Fig. 1. The bottom, the middle, and the top layers are the base beam, viscoelastic damping layer, and constraining layer, respectively. The 10-DOF beam element assumes that the base beam and the constraining layer satisfy the Bernoulli–Euler beam theory and undergo the same transverse and rotational deformations and that the viscoelastic damping layer has an additional shear angle associated with nonnegligible transverse shear. A brief explanation of the finite element formulation will be given here; a detailed formulation can be found in [11]. By considering the kinematic conditions of the displacements for the constrained-layer damping beam and applying the virtual work principle and discretizing the resulting equation using the finite elements, one can define the eigenvalue problem of the constrained-layer damping beam problem as

$$\mathbf{K}\mathbf{y} = \lambda^c \mathbf{M}\mathbf{y} \tag{1}$$

where $\mathbf{M}$ and $\mathbf{K}$ represent the global mass and stiffness matrices, respectively; $\mathbf{y}$ is the complex eigenvector; and λ^c is the complex eigenvalue. It should be noted that the stiffness matrix $\mathbf{K}$ becomes a complex-valued and frequency-dependent matrix due to the viscoelastic damping layer. To solve the frequency-dependent eigenvalue problem, the resubstitution method [12] is used. The ith eigenvector $\mathbf{y}_i$ satisfies the orthogonal conditions of the form

$$\mathbf{y}_i^T \mathbf{M}\mathbf{y}_j = \delta_{ij} m_j \tag{2}$$

$$\mathbf{y}_i^T \mathbf{K}\mathbf{y}_j = \delta_{ij} k_j \tag{3}$$

where δ_{ij} is the Kronecker delta and m_j and k_j are the generalized modal mass and the stiffness of the jth mode, respectively. The normalization condition that sets the mth component of the kth eigenvector (y_k^m) equal to one should also be imposed, where the

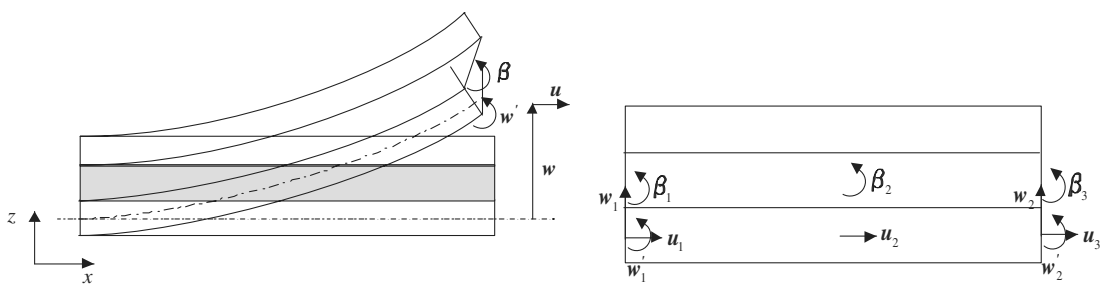

a) Displacements and sign conventions

b) Nodal degrees of freedom of the beam element

Fig. 1 Ten-DOF finite element for a constrained-layer damping beam.

index m is the maximum component of the kth eigenvector in the absolute sense. The natural frequency ψ_k and the modal loss factor η_k of the kth mode are defined as

$$\psi_k = \sqrt{\frac{\mathrm{Re}(\lambda_k^c)}{2\pi}}, \qquad \eta_k = \frac{\mathrm{Im}(\lambda_k^c)}{\mathrm{Re}(\lambda_k^c)} \tag{4}$$

where Re and Im refer to the real and the imaginary parts of the argument, respectively. To calculate the forced responses of the constrained-layer damping beam, the modal superposition method is used [11].

An analytic design sensitivity formula for dynamic responses can be obtained by differentiating the modal superposition expression. Knowing the eigenvalues and eigenvectors, the generalized modal masses, and the derivatives of the mass and stiffness matrices, the design sensitivity formula can be evaluated with a few matrix operations. The details are in [11].

B. Fractional Derivative Model

Viscoelastic damping material is made of very long intertwined and crosslinked molecular chains, each containing thousands or even millions of atoms. The internal molecular interactions that occur during deformation in general and vibration in particular give rise to macroscopic properties such as stiffness and energy dissipation during cyclic deformation. The material properties of the viscoelastic material show highly frequency- and temperature-dependent characteristics. By introducing an accurate mathematical model for those dependencies, one can enhance the efficiency of the finite element analysis in dynamic problems. In this subsection, the mathematical models for frequency- and temperature-dependent viscoelastic material will be explained briefly.

The dynamic responses of viscoelastic material in a frequency domain can be represented by a complex modulus such as

$$\tilde{\sigma} = E^*\tilde{\varepsilon} = (E' + iE'')\tilde{\varepsilon} \tag{5}$$

where $\sim$ refers to the Fourier transform, and E' and E'' are the storage modulus and loss modulus, respectively. The complex modulus of the viscoelastic damping material is strongly dependent on temperature and frequency. From the temperature–frequency equivalence hypothesis, any two complex moduli at different temperatures have a relation such as

$$E^*(f_0, T_0) = E^*(f_1\alpha(T_1)) \tag{6}$$

where $f\alpha$ is the reduced frequency. Therefore, by preparing the master curve at a reference temperature T_0, one can use the shift factor α to predict the complex modulus at any given temperature T. In addition, the shift factor and temperature in absolute degrees can be related by the Arrhenius equation as

$$\log[\alpha(T)] = d_1(1/T - 1/T_0) \tag{7}$$

Assuming a homogeneous isotropic material and linearity with respect to vibration amplitudes, the constitutive equation of the fractional derivative model of order one can be written as

$$\sigma(t) + c_1 D^\beta \sigma(t) = a_0\varepsilon(t) + a_1 D^\beta \varepsilon(t) \tag{8}$$

where $0 < \beta < 1$, and D^β indicates the fractional derivative [17]. The complex modulus of the viscoelastic damping material following the fractional derivative model can be obtained through the Fourier transforms of Eq. (8) and comparing the resulting equation with Eq. (5) in the case of extensional deformation as follows:

$$E^* = (E' + iE'') = \frac{a_0 + a_1[if\alpha(T)]^\beta}{1 + c_1[if\alpha(T)]^\beta} \tag{9}$$

where frequency is replaced by reduced frequency from the temperature–frequency equivalence hypothesis. The four material parameters a_0, a_1, c_1, and β are identified by minimizing the differences between the test data and the fractional derivative model [17]. Additionally, the parameters satisfy thermodynamic restrictions of the fractional derivative model [20]: 1) all parameters are positive and 2) a_1/c_1 is larger than a_0. In most cases, the viscoelastic damping material has one peak for the loss factor along frequencies. For the one-peak material, it is known that the four-parameter fractional derivative model sufficiently represents the real behavior of viscoelastic material over a wide frequency range [21]. Finally, it is evident that the complex modulus expression of Eq. (9) can be applied to the shear modulus in the same way, as can Young's modulus. Therefore, in this paper the complex Young's modulus and complex shear modulus will not be distinguished in symbols hereafter.

III. Characterization of Variability in the Viscoelastic Damping Layer

The constrained-layer damping performance is related to the dynamic properties of the viscoelastic damping material. However, the dynamic properties of the damping material are highly sensitive to changes in environmental temperature and/or the chemical composition of the material. RBDO can consider such variations in the process of design optimization so that one can obtain a robust design of the damping-layer layout even with extreme variability in the dynamic properties of the damping material. However, no systematic approach for identifying the variability in damping materials under environmental temperature change and/or composition uncertainty has been proposed. The authors propose a sound statistical approach to characterize the variability of the viscoelastic damping material for RBDO of the constrained-layer damping layout. This section presents the decomposition of the variability in the viscoelastic damping material into inherent variability and error in the complex modulus of the viscoelastic damping material.

A. Decomposition of Variability in Viscoelastic Damping Material

The variability in the dynamic responses of the viscoelastic damping material is primarily due to two sources: 1) operational temperature variation and 2) experimental/model errors associated with the viscoelastic damping material. When the damping layer is exposed to environmental air, operational temperature fluctuation causes substantial variation in the dynamic responses of the viscoelastic damping material, which can be observed through the Arrhenius equation in Eq. (7). In addition, errors in experimental data and mathematical models are inevitable in characterizing the viscoelastic damping material. The experimental errors include experiment noise and measurement inaccuracy. In addition, the mathematical models, such as the fractional derivative model, also introduce approximation errors because the models idealize and simplify the complicated behaviors of the viscoelastic damping material. It is extremely difficult to distinguish the model error from the experimental error unless the mathematical models are perfect or the experimental data is sufficiently given. To characterize the variability in the viscoelastic damping material properties, the complex modulus of the viscoelastic damping material can be expressed as

$$\begin{aligned} E^*(f,T) &= E_1^*(f,T) + \varepsilon_E^*(f) = E_1^*(f,T) \\ &\quad + (E_2^*(f,T_0) - \bar{E}_2^*(f,T_0)) \end{aligned} \tag{10}$$

where $E^*(f,T)$ indicates the uncertain complex modulus of the viscoelastic damping material considering the operational temperature variability and experiment/model errors (or uncertainty). The uncertain complex modulus can be decomposed into two terms: the random complex modulus E_1^* and the error (or uncertainty) in the complex modulus ε_E^*. The random complex modulus considers the operational temperature variability. From a set of test data over a concerned frequency range, the fractional derivative model gives a master curve of the complex modulus, which is a function of frequency at a given reference temperature T_0. Operational temperature fluctuation results in variations of the shift factor and the master curve in Eqs. (7) and (9). The variation of the master curve due to temperature fluctuation indicates the random complex modulus E_1^*.

In contrast, the error in the complex modulus is primarily due to experiment/model errors at a given temperature. Because of the experiment/model errors, there is random noise (or uncertainty) in the master curve of the complex modulus. In Eq. (10), $\bar{E}_2^*(f, T_0)$ is the mean of the master curve and $E_2^*(f, T_0)$ is the uncertain master curve due to the experimental/model errors. Thus, the error in the complex modulus can be defined as

$$\varepsilon_E^*(f) = E_2^*(f, T_0) - \bar{E}_2^*(f, T_0)$$

It is assumed that $\varepsilon_E^*(f)$ follows a Gaussian process and the experimental/model errors are dependent on frequency but not on operational temperature.

In this study, the variability of E_1^* and ε_E^* is sought to characterize the variability in the uncertain complex modulus, $E^*(f, T)$, based on the Arrhenius equation and the fractional derivative model. In Sec. III.B, the method used to characterize $E_1^*(f, T)$ with hourly temperature data is presented. In Sec. III.C, we propose a statistical approach for ε_E^* characterization based on a confidence interval (CI) on the master curve. In Sec. III.D, the proposed approach for variability characterization of the damping material is demonstrated with the viscoelastic damping material (ISD-110 [17]) and the material test (or experimental) data of the complex shear modulus.

B. Random Complex Modulus Because of Operational Temperature

For the characterization of the first term, $E_1^*(f, T)$, hourly temperature data measured for 1 year (2007) in Seoul was selected as a typical example of temperature variation. Figure 2 shows the temperature histogram generated from the temperature fluctuation in Seoul. Three temperature levels, mean μ_T and ± 3-sigma levels $\pm 3s_T$ are displayed in Fig. 2. It should be noted that the histogram shows a bimodal distribution. Figure 3 displays a rough estimate of the variability in the storage shear modulus and loss factor for the viscoelastic damping material (ISD-110) due to the temperature variation. Using the fractional derivative model, three curves in Fig. 3 are generated for the shift factor values corresponding to the three different temperature levels (μ_T and $\pm 3s_T$). One can see that the storage shear modulus and loss factor vary significantly due to the temperature variation, and the variation of the material properties can affect the dynamic responses of the constrained-layer damping structure.

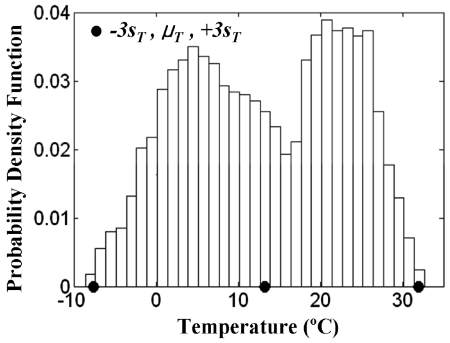

Fig. 2 Temperature histogram of Seoul in 2007.

C. Error in Complex Modulus Because of Experimental/Model Errors

This section presents a method to characterize the variability of the second term, ε_E^*, in Eq. (10), which requires estimating the variability of the parameters of the complex modulus due to experimental/model errors. To do so, the first step is to determine an unbiased estimator of the variance and the confidence interval (CI) for the master curve. The second step is to obtain the statistical information for the parameters of the complex modulus. This study employs a confidence level of 95%. A set of material test data of viscoelastic damping material, the master curve for the complex modulus, and mean values for the parameters of the complex modulus are required for characterization of ε_E^*. We use information on the complex shear modulus of ISD-110 given in [17].

First, the unbiased estimator of the variance for the master curve is calculated to construct the CI for the master curve. The residual sum of the squares between the observed value (z_i) and the fitted value on the master curve ($\hat{z}_i$) can be determined [22] as

$$SS_E = \sum_{i=1}^{q} (z_i - \hat{z}_i)^2 = \sum_{i=1}^{q} e_i^2 = \mathbf{e}^T \mathbf{e} \tag{11}$$

where q is the number of test data, e_i is the residual value for ith test data, and the vector of residuals is denoted by $\mathbf{e} = \mathbf{z} - \hat{\mathbf{z}}$. Thus, the unbiased estimator of the variance, $\hat{s}^2$, is given by

$$\hat{s}^2 = \frac{SS_E}{q - l} \tag{12}$$

where l is the number of regression coefficients and $q - l$ indicates the degrees of freedom associated with SS_E. The CI of the master curve can be obtained over a concerned frequency region using the following formulas:

$$E_{2.5\%}^* = \bar{E}_2^*(f, T_0) - 1.96\hat{s}, \quad E_{97.5\%}^* = \bar{E}_2^*(f, T_0) + 1.96\hat{s} \tag{13}$$

Here, the errors between the observed complex modulus value z_i and the fitted value $\hat{z}_i$ are assumed to be normally distributed with a zero mean.

The next step is to estimate the statistical information (e.g., CI) for the model parameters of the complex modulus over a specified frequency range. The statistical information can be extracted by analyzing the physical meanings of the fractional derivative model parameters (a_0, a_1, c_1, and β). First, the parameter $\log(a_0)$ is equal to the estimated logarithmic value of the storage modulus in the range of low frequency. Thus, the variance of the parameters $\log(a_0)$ can be directly characterized with the CI of the master curve using the following formula:

$$s_{\log(a_0)} = \frac{\log(a_0)_{97.5\%} - \overline{\log(a_0)}}{1.96} \tag{14}$$

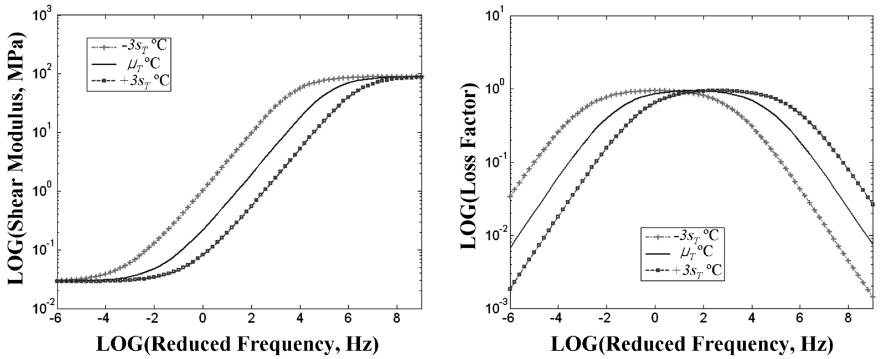

Fig. 3 Variability of material properties due to temperature variation.

where $s_{\log(a0)}$ is the standard deviation of $\log(a_0)$; $\log(a_0)_{97.5\%}$ is obtained from the $E^*_{97.5\%}$ curve at low frequency (10^{-6} Hz); and $\overline{\log(a_0)}$ is the mean value of $\log(a_0)$. Knowing that the parameter β represents the slope of the plot of $\log(E')$ versus $\log(f\alpha)$ in a transition region, the variation of the parameter β can be estimated by calculating the unbiased estimator of the variance of the slope. Finally, the ratio of the parameters a_1/c_1 represents the asymptotic value of the storage modulus at very high frequencies, as one can see in Eq. (9). Therefore, the variation of $\log(a_1/c_1)$ can be estimated from the variation of the storage modulus in the range of high frequency. It should be noted that the two parameters $\log(a_1)$ and $\log(c_1)$ are statistically correlated. The mean values of the parameters are given from the master curve. To characterize the joint probability density function (PDF) of $\log(a_1)$ and $\log(c_1)$, an allowable set of two parameters, $\log(a_1)$ and $\log(c_1)$, can be constructed by identifying the random samples that sit in the 95% CI of the master curve at high frequency. The random samples are obtained by assuming that the variations of two parameters are the same as that of $\log(a_0)$. A correlation matrix can be constructed to represent the statistical correlation of the two parameters. The correlation matrix can be approximated by defining the following eigenvalue problem as

$$\mathbf{A}\mathbf{v} - \lambda\mathbf{v} = 0, \qquad \mathbf{A} = \begin{bmatrix} a_{11} & a_{12} \\ a_{21} & a_{22} \end{bmatrix} \tag{15}$$

where $\mathbf{A}$ is the covariance matrix, and λ and $\mathbf{v}$ are the eigenvalues and eigenvectors, respectively. Here, the covariance matrix $\mathbf{A}$ is unknown. Instead, the allowable set of their realization can approximate the eigenvalues and eigenvectors of the covariance matrix and build the covariance matrix $\mathbf{A}$. The variances s^2 and the correlation coefficient ρ of the parameters $\log(a_1)$ and $\log(c_1)$ can be calculated by the following relation as

$$s^2_{\log(c_1)} = a_{11}, \qquad s^2_{\log(a_1)} = a_{22}, \qquad \rho_{\log(c_1),\log(a_1)} = \frac{a_{12}}{\sqrt{a_{11}} \cdot \sqrt{a_{22}}} \tag{16}$$

The procedure with the viscoelastic damping material (ISD-110) will be explained in detail in the next subsection.

D. Variability Characterization of the Viscoelastic Damping Material (ISD-110)

The proposed method to estimate the variability of damping material due to operational temperature and experimental/model errors was applied to a damping material, ISD-110. The 3M damping material ISD-110 is a typical damping adhesive usually used in constrained-layer damping. This study employs material test data on ISD-110 taken from sandwich beam tests in [17]. The test data include the storage shear moduli and loss factors at different frequencies and corresponding shift factors. From the test data, the parameters of the complex modulus are estimated, as is the master curve at a reference temperature T_0. The variability of $E^*_1(f,T)$ can be characterized through uncertainty propagation using Monte Carlo simulation (MCS), which employs Eqs. (7) and (9). Likewise, the variability of $\varepsilon^*_E(f)$ can also be characterized using the statistical approach explained in Secs. III.B and III.C. The uncertainty characterization procedure for the viscoelastic damping material (ISD-110) is shown in Fig. 4.

Following the proposed method, the variation of shift factor for ISD-110 is first obtained. The temperature information in Seoul is used for operational temperature, as shown in Fig. 2. The variability in the temperature profile results in the uncertainty of the Arrhenius shift factor in Eq. (7). The shift factor is a function of both operational temperature T and the material constant d_1. However, the uncertainty of d_1 is not considered due to its negligible effect on the shift factor. This is confirmed by comparing the histograms of the shift factor with and without corresponding d_1 variance. Figure 5 shows the histogram of the shift factor due to the temperature change only. Table 1 shows the estimated statistical information of temperature, d_1, and $\log(\alpha)$.

Next, for ε^*_E, the proposed statistical approach is applied to the material test data of ISD-110. Figure 6a shows the log–log plots of the material test data, the master curve (solid line), and 95% CI of the master curve calculated using Eq. (13) (dashed line) about the storage shear modulus of ISD-110. As shown in Fig. 6a, most of the storage shear modulus data are within the 95% CI. The variance of the parameter $\log(a_0)$ is obtained using Eq. (14). Similarly, the variation of the parameter β is also obtained from the test data in the transition region, $\log 10^{-0.5} - \log 10^{2}$ Hz. Figure 7 shows the test data in the transition region. The unbiased estimator of the variance for the

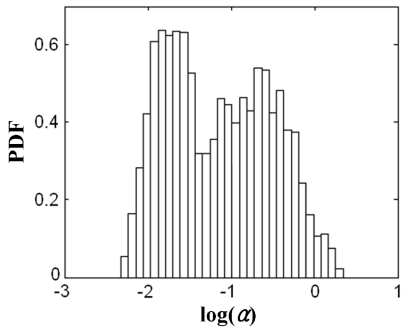

Fig. 5 Histogram of the shift factor.

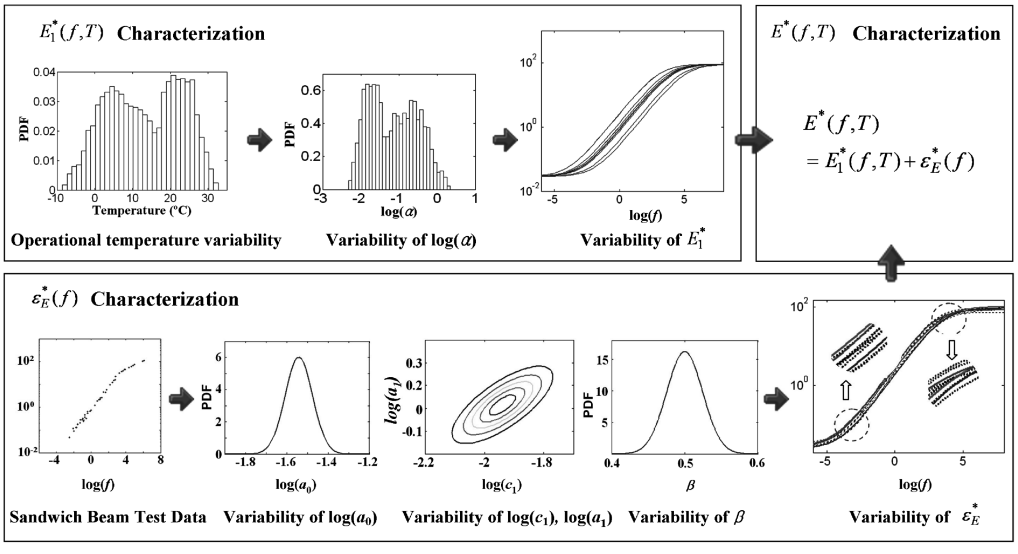

Fig. 4 Variability characterization procedure of viscoelastic damping material.

Table 1 Properties of random variables for constrained-layer damping performances (ISD-110 damping material and $\rho_{\log(c1),\log(a1)} = 0.7349^*$)

Random variable	Mean	Standard deviation	Distribution type
Temperature, °C	13.28	9.79	Bimodal data
d_1	5224	54	Normal
$\log(\alpha)$	−1.14	0.63	Bimodal
$\log(a_0)$	log(0.0287)	0.0663	Normal
$\log(a_1)$	log(1.0350)	0.0913	Normal
$\log(c_1)$	log(0.0115)	0.0913	Normal
β	0.5	0.0246	Normal

parameter β is obtained from the residual sum of squares between the linear regression model and the test data using Eqs. (11) and (12). The linear regression model and 95% CI for the parameter β are also shown in Fig. 7.

Finally, the variances and the correlation coefficient of the parameters $\log(a_1)$ and $\log(c_1)$ are characterized. It is assumed that the $\log(a_1/c_1)$ is normally distributed, as are the $\log(a_1)$ and $\log(c_1)$. Figure 8 shows the allowable combinations of the parameters $\log(a_1)$ and $\log(c_1)$, which sit in the 95% CI of Fig. 6a over the specified frequency range. Because the value of $\log(a_1/c_1)$ is equal to the asymptotic logarithmic value of the storage shear modulus in the range of high frequency, $\log(a_1)$ is linearly proportional to $\log(c_1)$. In other words, $\log(a_1/c_1) = \text{constant}$ or $\log(a_1) = \log(c_1) + \text{constant}$. Therefore, the principal directions of the anticipated joint PDF are [−1, 1] and [1, 1]. The hexagon that encompasses all the allowable combinations is obtained based on the principal directions for joint PDF approximation. The set of allowable combinations appears to maintain the symmetry of the joint PDF to the principal directions. Because the hexagon encompasses the allowable combinations found with 95% CI of Fig. 6a, the hexagon is considered to be the joint PDF with 95% confidence level. This process gives the eigenvalues of the joint PDF as follows:

$$\lambda_1 = s_1^2, \qquad \lambda_2 = s_2^2 \tag{17}$$

where s_1^2 and s_2^2 are the variances along the directions of the principal axes, respectively, and s_1 and s_2 are calculated by dividing the hexagon widths along the principal directions by 1.96. The joint PDF of $\log(a_1)$ and $\log(c_1)$ fitting the allowable combinations can be obtained by solving the eigenvalue problem in Eq. (15). The variances and the correlation coefficients of the parameters $\log(a_1)$ and $\log(c_1)$ are calculated using Eq. (16). The variability due to the experiment/model errors for the ISD-110 damping material is summarized in Table 1. The characterized variability is cross-validated with the test data on the loss factor of ISD-110. Figure 6b shows 95% CI of the master curve for the loss factor. The 95% CI is calculated using the variance of the characterized parameters of the complex modulus in Table 1. It is noted that most of the loss factor data also lie within the 95% CI. The characterized parameters are used for RBDO of the constrained-layer damping layout in Sec. IV.

E. Influence of Material Variability on System Response

To show the influence of the material variability on the dynamic response of a damping-layer structure, this study considers a simply supported beam problem (Fig. 9) with constrained-layer damping material. For the constrained-layer damping beam problem, the four parameters (a_0, a_1, c_1, and β) of the fractional derivative model and operational temperature (or shift factor α) are selected as the random variables, and their properties are listed in Table 1. The forced responses (point receptance frequency responses) are calculated at 1000 random samples of the random variables generated by MCS. Figure 10 shows the calculated variability bound (with 95% CI) of the forced response in a decibel scale over a specified frequency range. The magnitude of the amplitude variation at the peak is beyond 10 dB. It is true that the variability of the viscoelastic damping material causes large variability on the frequency response of the constrained-layer damping structure. This highlights the importance of the variability in the optimization of a damping-layer design.

IV. Reliability-Based Design Optimization of Constrained-Layer Damping Layout

A. Reliability-Based Design Optimization Formulations

The design objective of a constrained-layer damping treatment is to maximize the robustness and meet a reliability target while using a minimal amount of the damping layer. The simply supported aluminum beam structure with constrained-layer damping in Fig. 9 is considered for demonstration purposes. The ISD-110 damping material is used for the damping layer of the structure. A unit force F

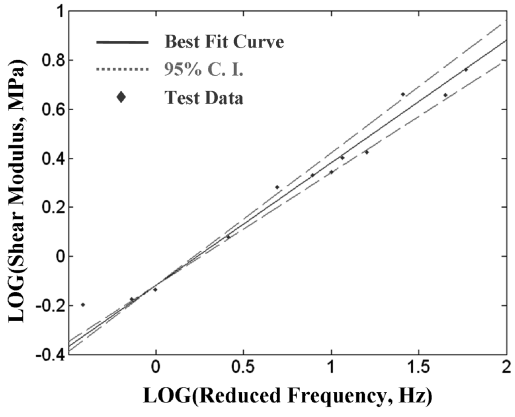

Fig. 7 Variability of the parameter β.

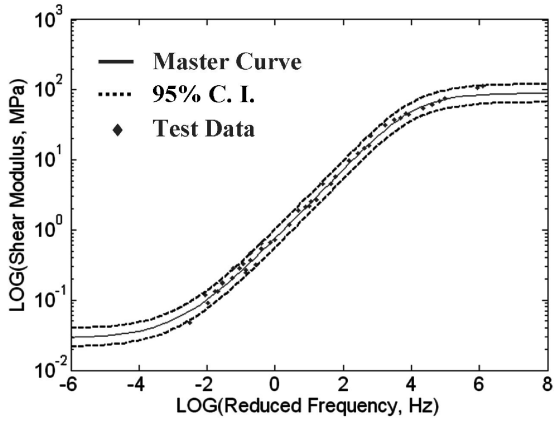

a) Storage shear modulus

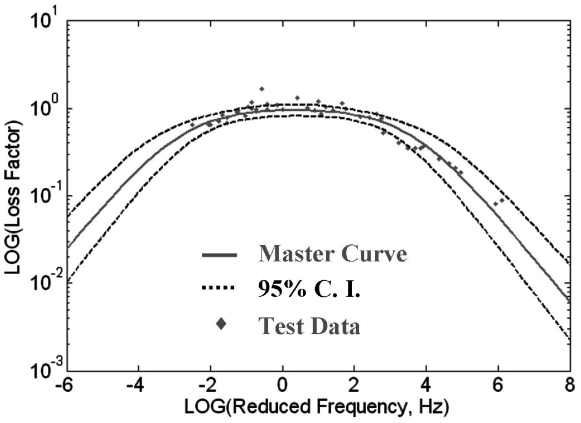

b) Loss factor

Fig. 6 Material properties of ISD-110 damping material.

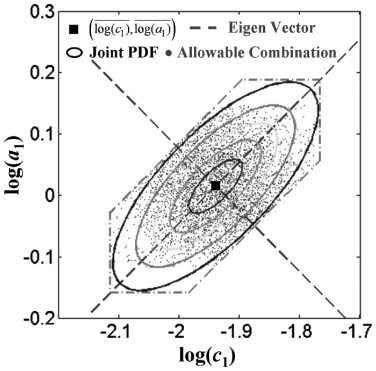

Fig. 8 Joint PDF for the parameters a_1 and c_1.

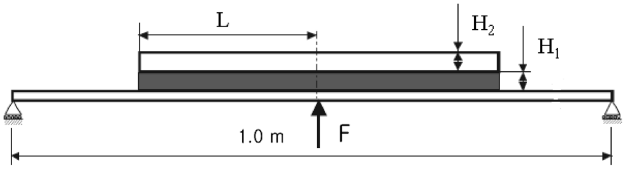

Fig. 9 Simply supported beam problem.

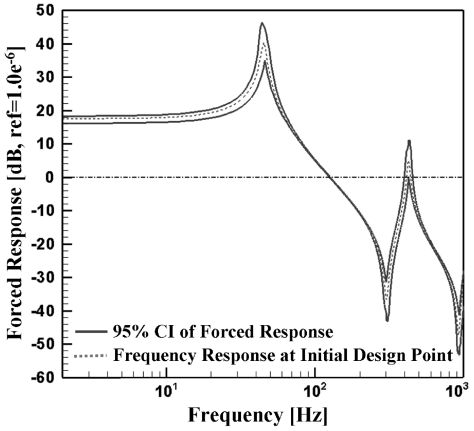

Fig. 10 Forced response variability of a constrained-layer damping beam problem.

is applied to the center of the aluminum beam and the thickness of the base beam is 20 mm.

The beam structure has three design variables: the length of the constrained layer (L) and the thicknesses of the damping layer (H_1) and the constraining layer (H_2). The thickness of the base beam remains constant during the optimization. The random variables for the constrained-layer damping performance shown in Table 1 are used in this optimization problem. Additionally, the manufacturing variability of the design variables is also considered in the RBDO formulation. As listed in Table 2, their coefficients of variations (COVs) are assumed to be 1, 10, and 5%, respectively.

Table 2 Design variable of the beam structure

Design variable	Initial value	Lower bound	Upper bound	COV	Distribution type
L, m	0.2	0.1	0.45	1%	Normal
H_1, mm	0.5	0.1	3	10%	Normal
H_2, mm	5	1	10	5%	Normal

The RBDO problem can be formulated as

$$\begin{aligned} &\text{minimize } \Phi(\mathbf{b};\mathbf{X}) \qquad \text{subject to } P(G_i(\mathbf{b};\mathbf{X})\langle 0\rangle)R^t \\ &i=1,\ldots,np \qquad \mathbf{b}^L \le \mathbf{b} \le \mathbf{b}^U, \mathbf{X}^L \le \mathbf{X} \le \mathbf{X}^U \end{aligned} \tag{18}$$

where $\mathbf{b}$ is the design variable vector, $\mathbf{X}$ is the random variable vector, Φ is the objective function, $P(\cdot)$ indicates probability, G is the constraint function, np is the number of constraints, and R^t is the target reliability (99.865%, 3-sigma level). The RBDO formulation minimizes the mean and standard deviation of the objective function for system robustness.

In general, the objective and the constraint functions can be differently formulated to meet various design objectives or requirements. Three design performances are used to represent design objectives or requirements as

$$\begin{aligned} \Pi_1(\mathbf{b}) &= W \qquad \Pi_2(\mathbf{b},\mathbf{X}) = \int_{f_1}^{f_2} \left\langle 20\log\frac{\|\zeta\|}{\zeta_{\text{ref}}} - \zeta_{dB0} \right\rangle \mathrm{d}f \\ \Pi_3(\mathbf{b},\mathbf{X}) &= \eta_1 + \eta_3 \end{aligned} \tag{19}$$

where ζ is the forced response function (point receptance frequency response function) at the center point and $\langle\zeta\rangle$ is defined as

$$\langle\zeta\rangle = \begin{Bmatrix} \zeta & \text{if } \zeta > 0 \\ 0 & \text{if } \zeta \le 0 \end{Bmatrix} \tag{20}$$

ζ_{ref} is $1.0 \times \text{E} - 6$, and ζ_{dB0} is a prescribed level in the decibel scale. The first function, $\Pi_1(\mathbf{b})$, is the weight performance in the constrained-layer damping structure, where the weight is defined as

$$W = 2 \cdot L \cdot (w_1 \cdot H_1 + w_2 \cdot H_2) \cdot \xi \tag{21}$$

where w_1 and w_2 are the densities of damping and constraining layers, respectively, and ξ is the width of the beam structure. The second function, $\Pi_2(\mathbf{b},\mathbf{X})$, is the overall damping performance, which corresponds to the area of the forced response not beyond a target value in the decibel scale over a specified frequency range. The smaller $\Pi_2(\mathbf{b},\mathbf{X})$ indicates more damping and response abatement. The third function, $\Pi_3(\mathbf{b},\mathbf{X})$, is the modal damping performance that corresponds to the sum of the loss factors at the first and third structural modes. The greater $\Pi_3(\mathbf{b},\mathbf{X})$ indicates more modal damping.

Three different design formulations have been commonly used in a deterministic form [4,11]. Therefore, we used three RBDO formulations for the constrained-layer damping problem, as summarized in Table 3. The first RBDO problem is formulated to maximize the damping performance (design objective) and to meet the weight performance requirement (design requirement). Here, the constraint means that the added weight due to the constrained-layer damping should be less than 5% of the base-beam weight. It should be noted that the probability constraint of formulation I is not dependent on the variability in the damping material properties and operation temperature, but dependent only on the manufacturing variability. Thus, another possible formulation that maximizes the modal damping performance ($\Pi_3(\mathbf{b},\mathbf{X})$) under the weight constraint

Table 3 Optimization formulations for the constrained-layer damping layout design

	Formulation I	Formulation II	Formulation III
Design variables	$\mathbf{b} = \{L \quad H_1 \quad H_2\}^T$	$\mathbf{b} = \{L \quad H_1 \quad H_2\}^T$	$\mathbf{b} = \{L \quad H_1 \quad H_2\}^T$
Objective function Φ	$\Pi_2(\mathbf{b},\mathbf{X})$	$\Pi_1(\mathbf{b})$	$\Pi_1(\mathbf{b})$
Constraint function[a]	$G_1 = \Pi_1 - W_b \cdot G^t < 0$, where $G^t = 0.05$	$G_2 = \Pi_2 - \Pi_{20} \cdot G^t < 0$, where $G^t = 0.90$	$G_3 = G^t - \Pi_3 < 0$, where $G^t = 0.15$

[a] W_b is the base beam weight, Π_{20} is the functional value of Π_2 at initial design, and G^t refers to the target constraint value.

Table 4 Optimization results of formulation I

	Initial	DDO	RBDO
Design variable			
L, m	0.2000	0.1180	0.1026
H_1, mm	0.5000	0.1000	0.1000
H_2, mm	5.0000	4.2025	4.1901
Object function	41,453	46,108	47,689
Reliability			
EDR	0%	50%	99.865%
MCS	——	——	99.82%

is not considered in the formulation set. On the other hand, the second and third problems are formulated to minimize the weight performance (design objective) to meet the damping performance requirement (design requirement). In the second and third RBDO formulations, the different constraint forms treat the damping performance requirement differently. In formulation II, the constraint means that the area generated by response graph should be reduced by 10% than that of initial design. In formulation III, the constraint forces the summation of the modal loss factors to be larger than the constraint target value, 0.15.

B. Uncertainty Propagation and Probability Analysis

The eigenvector dimension reduction (EDR) method [18] is used for effectively building probability distributions for the dynamic responses of a damping layer. The EDR method is an enhanced version of the univariate dimension reduction (DR) method [23]. The univariate DR method estimates the statistical moments of a system response using an additive univariate decomposition of the response. Statistical moments of the response, $Y(\mathbf{X})$, can be calculated as

$$E\{Y^m(\mathbf{X})\} = \int_{-\infty}^{\infty} \int_{-\infty}^{\infty} Y^m(\mathbf{x}) \cdot p_{\mathbf{x}}(\mathbf{x}) \cdot \mathrm{d}\mathbf{x}, \qquad m = 0, 1, 2, \ldots \tag{22}$$

where E indicates an expectation operator and $p_{\mathbf{x}}(\mathbf{x})$ is the joint PDF of $\mathbf{X}$. Multidimensional integration in Eq. (22) can be converted into multiple one-dimensional integrations using an additive decomposition. Using the binomial formula, multiple one-dimensional integration can be solved recursively. Any numerical integration scheme can be used to perform one-dimensional integration.

To enhance both accuracy and efficiency in probability analysis, three technical elements are used in the EDR method:

1) The eigenvector sampling method is used to resolve correlated and asymmetric random input variables.

2) The stepwise-moving least-squares method is used for one-dimensional response approximation.

3) A stabilized Pearson system is used to generate a PDF of a system response.

Thus, for N number of random variables, the EDR method demands $2N + 1$ or $4N + 1$ eigenvector samples at which system responses are computed using simulations or experimental tests. The detailed procedure of the EDR method is explained in [18].

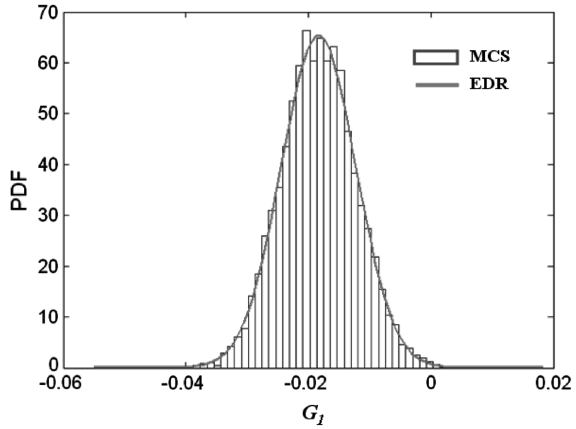

Fig. 11 MCS histogram and EDR PDF at the optimum design for formulation I.

C. Design Optimization Result

The RBDO problems are solved using our in-house RBDO software along with an `fmincon` function in MATLAB software [24] as a gradient-based optimizer. The finite element (FE) formulation is employed to calculate the frequency responses of the constrained-layer damping beam problem, and a continuum design sensitivity analysis is used to compute their sensitivities for design optimization. The constrained-layer damping beam is modeled with 20 elements using the 10-DOF finite elements for the constrained part and the degenerated elements for the bare part. The EDR method uses $4N + 1$ FE analysis calls for estimating the objective function and constraint in a probabilistic manner. The target reliability for the all design formulations is set to 99.865% (3-sigma level). The deterministic design optimization (DDO) is first performed and followed by RBDO starting from the deterministic optimal design points. RBDO uses the statistical information of the random variables shown in Tables 1 and 2, and the corresponding RBDO results are carefully compared in this study. To confirm the accuracy of the EDR method, MCS results are employed as benchmark solutions.

Formulation I is preferred when weight is constrained in the design of the constrained-layer damping layout. Table 4 shows the results of formulation I at the initial, deterministic, and reliability-based optimum design points. First, as shown in Fig. 11, the PDF of G_1

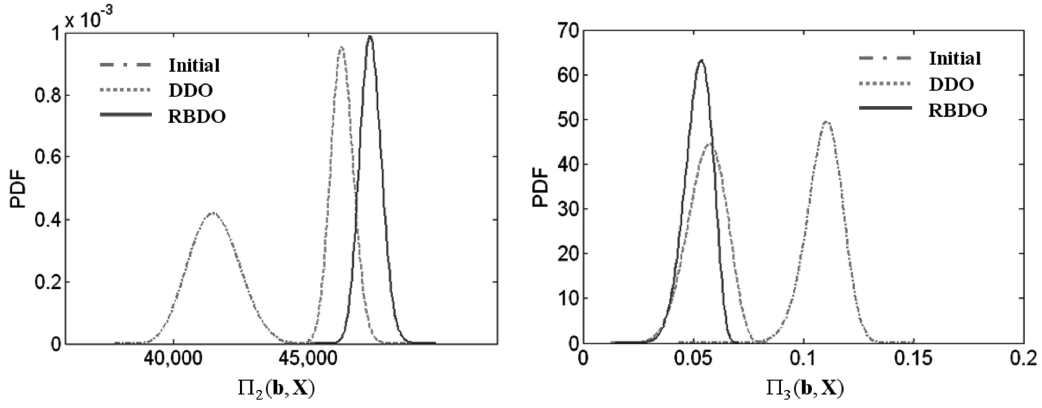

a) Overall damping performance **b) Modal damping performance**

Fig. 12 PDFs of the performance functions for formulation I.

Table 5 Optimization results of formulation II

	Initial	DDO	RBDO
Design variable			
L, m	0.2000	0.1753	0.1794
H_1, mm	0.5000	0.1000	0.1000
H_2, mm	5.0000	7.4684	8.7109
Object function	0.2857	0.3629	0.4520
Reliability			
EDR	0%	38.60%	99.865%
MCS	——	——	99.79%

Table 6 Optimization results of formulation III

	Initial	DDO	RBDO
Design variable			
L, m	0.2000	0.2837	0.3836
H_1, mm	0.5000	0.7975	1.0074
H_2, mm	5.0000	5.0313	5.2353
Object function	0.2857	0.4159	0.6188
Reliability			
EDR	0%	30.88%	99.865%
MCS	——	——	99.92%

from the EDR method is compared with the histogram from the MCS with 10,000 random samples. Uncertainty in the design variables precisely propagates to that of the constraint function G_1 through the EDR method. Table 4 confirms that the reliability is also predicted accurately. In Table 4, it is noted that the damping performance (design objective) is sacrificed by about 15% to improve the weight reliability (design requirement) by 99.865%. Figure 12 shows the overall and modal damping performances of three different designs (initial, deterministic optimum, and reliability-based optimum designs). It was found that a great deal of the infeasibility of the initial design forced the mean of the overall damping performance (design objective) to be sacrificed. Since the modal damping performance is not considered in formulation I, its variation is slightly reduced. However, significant reduction in the variation of the overall damping performance indicates greater robustness, which proves the usefulness of this optimization formulation.

Formulation II is preferred when the overall damping performance is constrained in the design of constrained-layer damping layout. The optimization results of formulation II are listed in Table 5. Figure 13 shows the PDF of G_2 from the EDR method and the histogram from MCS with 10,000 random samples. The EDR method gives an accurate PDF and reliability with lower computational cost. The variability of G_2 that is propagated from the variability of temperature, the experimental/model error, and the design variables is around 10% of the mean value of G_2. As found in Table 5 and Fig. 14a, the deterministic optimum design turns out to be unreliable (38.5%) due to the variability of G_2. This underscores the strong need to consider the uncertainties in the design of constrained-layer damping layout. A deterministic optimum design tends to have about 50% reliability; however, 38.5% reliability is mainly due to bimodal temperature variability. The weight performance (design objective) is sacrificed by about 58.2% to improve the reliability of the overall damping performance (design requirement) by 99.865%. Figure 14 shows the PDFs of the overall and modal damping performances at the initial, deterministic, and reliability-based optimum design points. The overall damping performance (design requirement) is considerably improved, as shown in Fig. 14a; however, the modal damping performance becomes substantially worse in terms of its variation since it is not considered in formulation II. Figure 15 shows the forced responses at three different design points for formulation II. The design requirement (damping performance) becomes reliable by moving the resonant frequencies to higher (or reducing the overall damping performance) rather than by reducing the amplitude at the first and third resonance frequencies (the modal damping performance). That is mainly because formulation II considers the overall damping performance.

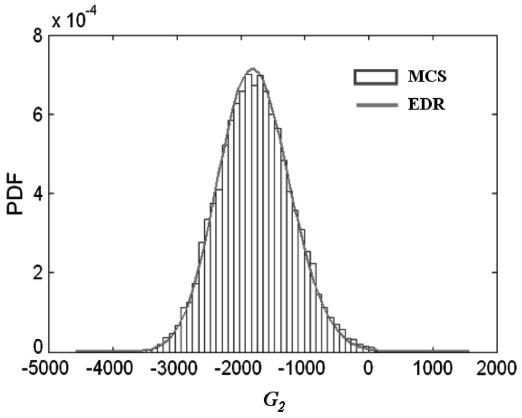

Fig. 13 MCS histogram and EDR PDF at the optimum design for formulation II.

Formulation III is used when modal loss factors are crucial in the design of constrained-layer damping layout. The optimization results of formulation III are listed in Table 6. As shown in Fig. 16, uncertainty in the design and the uncontrollable random variable precisely propagates to that of the constraint function, G_3, through the EDR method. The variability of G_3 is around 50% of the mean value of G_3. In Table 6, one can also see that the deterministic optimum design is unreliable (30.88%) due to the variability of G_3. The weight performance (design objective) is sacrificed by about 116.6% to improve the reliability of the modal damping performance (design requirement) by 99.865%. Figure 17 shows the PDFs of the

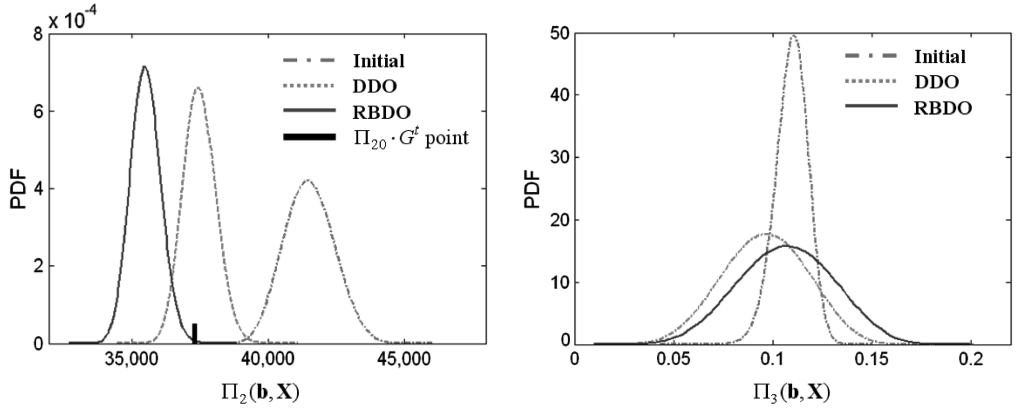

a) Overall damping performance **b) Modal damping performance**

Fig. 14 PDFs of the performance functions for formulation II.

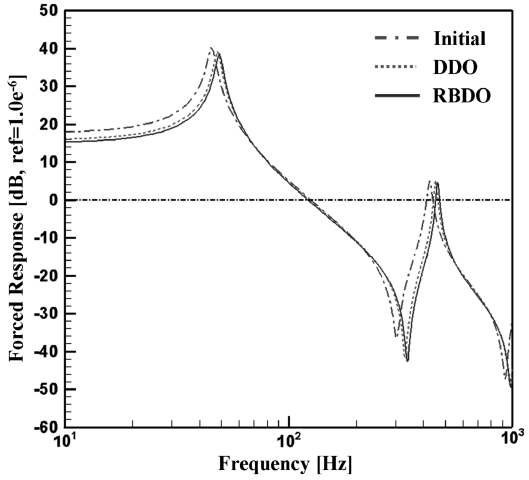

Fig. 15 Forced responses at the optimum design for formulation II.

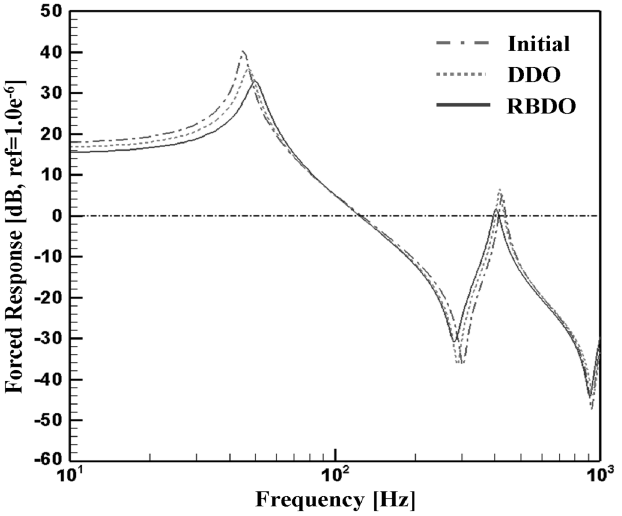

Fig. 18 Forced responses at the optimum design for formulation III.

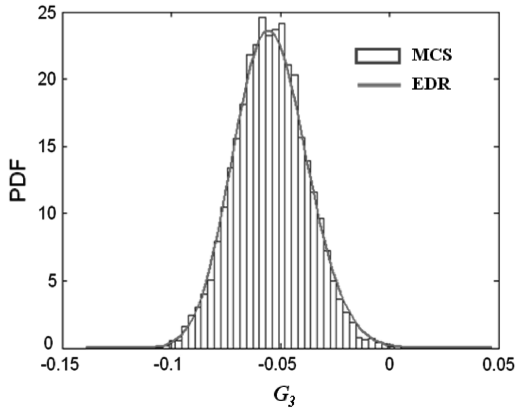

Fig. 16 MCS histograms and EDR PDF at the optimum design for formulation III.

overall and modal damping performance at the initial, deterministic, and reliability-based optimum design points. The overall and modal damping performances are considerably enhanced in terms of their mean values. However, the variation of the modal damping performance slightly increases in terms of its variation, which is far better than the result of formulation II (see Fig. 14b). Figure 18 shows the forced responses at three different design points for formulation III. The design requirement (the modal damping performance) becomes reliable by reducing the amplitude at the first and third resonance frequencies.

V. Conclusions

This paper proposed a statistical approach 1) to model variability of viscoelastic damping material in a constrained-layer damping layout, 2) to predict variability in the dynamic responses of viscoelastic damping material, and 3) to obtain an optimal robust layout amidst severe variability in operational temperature. Variability in the viscoelastic damping material property can be decomposed into a random complex modulus due to operational temperature variability and experiment/model errors in the complex modulus. The variability of operational temperature was characterized with hourly measured temperature data and was propagated through the Arrhenius equation to the variability in the dynamic responses of viscoelastic damping material. A statistical approach was suggested for the variability characterization of experiment/model errors in the complex modulus. The EDR method was used to predict the variability in the material properties of viscoelastic damping material and operational temperature. The result of the probability analysis demonstrated that temperature variability is strongly propagated to that in the dynamic responses of the damping material. The characterized variability of dynamic responses enables a robust design optimization of the constrained-layer damping structure. In this study, three RBDO formulations were employed to meet various design objectives or requirements. In formulation I, the damping performance (design objective) was sacrificed by about 15% to improve the weight reliability (design requirement) by 99.865%. Therefore, this design formulation is preferred when weight is constrained in the design of constrained-layer damping layout. On

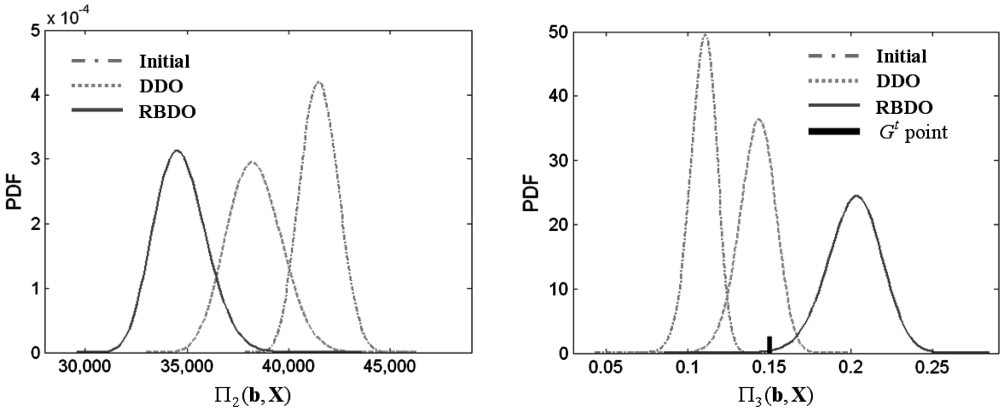

a) Overall damping performance **b) Modal damping performance**

Fig. 17 PDFs of the performance function for formulation III.

the other hand, formulations II and III increased the weight (design objective) by 58.2 and 116.6%, respectively, while improving the reliability of their damping performances (overall damping for formulation II and modal damping for formulation III) by 99.865%. Hence, these design formulations are more suitable when damping performances are constrained in the design of constrained-layer damping layout. It is not meaningful to make direct comparisons between formulations II and III because the results depend on their target constraint values. Overall, it is shown that the proposed approach results in robust and reliable damping layout designs amidst severe variability in operational temperature.

Acknowledgments

This work was supported by U.S. National Science Foundation (NSF) under grant no. GOALI-0729424; U.S. Army Tank and Automotive Research, Development and Engineering Center under the Short Term Analysis Study contract (TCN-05122); General Motors under grant no. TCS02723; and a Dongeui University Foundation grant (2008).

References

[1] Rao, M. D., "Recent Applications of Viscoelastic Damping for Noise Control in Automobiles and Commercial Airplanes," *Journal of Sound and Vibration*, Vol. 262, No. 3, 2003, pp. 457–474. doi:10.1016/S0022-460X(03)00106-8

[2] Wins, D. J., *Modal Testing: Theory, Practice and Application*, Research Studies Press, Bal Dock, England, U.K., 2000.

[3] Lall, A. K., Nakra, B. C., and Asnani, N. T., "Optimum Design of Viscoelastically Damped Sandwich Panels," *Engineering optimization*, Vol. 6, No. 4, 1983, pp. 197–205. doi:10.1080/03052158308902470

[4] Lifshitz, J. M., and Leibowitz, M., "Optimal Sandwich Beam Design for Maximum Viscoelastic Damping," *International Journal of Solids and Structures*, Vol. 23, No. 7, 1987, pp. 1027–1034.

[5] Marcelin, J. L., Trompette, P., and Smatic, A., "Optimal Constrained Layer Damping with Partial Coverage," *Finite Elements in Analysis and Design*, Vol. 12, No. 3, 1992, pp. 273–280. doi:10.1016/0168-874X(92)90037-D

[6] Baz, A., and Ro, J., "Optimum Design and Control of Active Constrained Layer Damping," *Journal of Mechanical Design*, Vol. 117, No. 2, 1995, pp. 135–144. doi:10.1115/1.2836447

[7] Nakra, B. C., "Vibration Control in Machines and Structures Using Viscoelastic Damping," *Journal of Sound and Vibration*, Vol. 211, No. 3, 1998, pp. 449–465. doi:10.1006/jsvi.1997.1317

[8] Zheng, H., Cai, C., and Tan, X. M., "Optimization of Partial Constrained Layer Damping Treatment for Vibrational Energy Minimization of Vibrating Beams," *Computers and Structures*, Vol. 82, Nos. 29–30, 2004, pp. 2493–2570. doi:10.1016/j.compstruc.2004.07.002

[9] Kim, T. W., and Kim, J. H., "Eigensensitivity Based Optimal Distribution of a Viscoelastic Damping Layer for a Flexible Beam," *Journal of Sound and Vibration*, Vol. 273, Nos. 1–2, 2004, pp. 201–218. doi:10.1016/S0022-460X(03)00479-6

[10] Zheng, H., and Cai, C., "Minimization of Sound Radiation from Baffled Beams Through Optimization of Partial Constrained Layer Damping Treatment," *Applied Acoustics*, Vol. 65, No. 5, 2004, pp. 501–520. doi:10.1016/j.apacoust.2003.11.008

[11] Lee, D. H., "Optimal Placement of a Constrained-Layer Damping for Reduction of Interior Noise," *AIAA Journal*, Vol. 46, No. 1, 2008, pp. 75–83. doi:10.2514/1.30648

[12] Lee, D. H., and Hwang, W. S., "Layout Optimization of an Unconstrained Viscoelastic Layer on Beams Using Fractional Derivative Model," *AIAA Journal*, Vol. 42, No. 10, 2004, pp. 2167–2170. doi:10.2514/1.7482

[13] Kareem, A., and Sun, W. J., "Dynamic Response of Structures with Uncertain Damping," *Engineering Structures*, Vol. 12, 1990, pp. 2–8. doi:10.1016/0141-0296(90)90032-N

[14] Kareem, A., and Gurley, K., "Damping in Structures: Its Evaluation and Treatment of Uncertainty," *Journal of Wind Engineering and Industrial Aerodynamics*, Vol. 59, Nos. 2–3, 1996, pp. 131–157. doi:10.1016/0167-6105(96)00004-9

[15] Li, J., and Chen, J., "Dynamic Response and Reliability Analysis of Structures with Uncertain Parameters," *International Journal for Numerical Methods in Engineering*, Vol. 62, No. 2, 2005, pp. 289–315. doi:10.1002/nme.1204

[16] Soize, C., "A Comprehensive Overview of a Non-Parametric Probabilistic Approach of Model Uncertainties for Predictive Models In Structural Dynamics," *Journal of Sound and Vibration*, Vol. 288, No. 3, 2005, pp. 623–652. doi:10.1016/j.jsv. 2005.07.009

[17] Jones, D. I. G., *Handbook of Viscoelastic Vibration Damping*, Wiley, New York, 2001, Chaps. 2–8.

[18] Youn, B. D., Xi, Z., and Wang, P., "The Eigenvector Dimension-Reduction (EDR) Method for Sensitivity-Free Uncertainty Quantification," *Structural and Multidisciplinary Optimization*, Vol. 37, No. 1, 2008, pp. 13–28. doi:10.1007/s00158-007-0210-7

[19] Youn, B. D., and Wang, P., "Bayesian Reliability-Based Design Optimization Using Eigenvector Dimension Reduction (EDR) Method," *Structural and Multidisciplinary Optimization*, Vol. 36, No. 2, 2008, pp. 107–123. doi:10.1007/s00158-007-0202-7

[20] Bagley, R. L., and Torvik, P. J., "On the Fractional Calculus Model of Viscoelastic Behavior," *Journal of Rheology (New York)*, Vol. 30, No. 1, 1986, pp. 133–155. doi:10.1122/1.549887

[21] Eldred, L. B., Baker, W. P., and Palazotto, A. N., "Kelvin-Voigt vs. Fractional Derivative Model as Constitutive Relations for Viscoelastic Material," *AIAA Journal*, Vol. 33, No. 3, 1995, pp. 547–550. doi:10.2514/3.12471

[22] Myers, R. H., and Montgomery, D. C., *Response Surface Methodology*, Wiley, New York, 1995, Chaps. 2–3.

[23] Rahman, S., Xu, H., "A Univariate Dimension-Reduction Method for Multi-Dimensional Integration in Stochastic Mechanics," *Probabilistic Engineering Mechanics*, Vol. 19, No. 4, 2004, pp. 393–408. doi:10.1016/j.probengmech.2004.04.003

[24] MATLAB, Software Package, Ver. 7.5.(R2007b), The Mathworks, Inc., Natick, MA, 2007.

A. Messac
Associate Editor